Enhancing the TAMU Model for Predicting Buckling in Rails

David H. Allen
Professor
Director, Center for Railway Research
Ocean Engineering Department
Texas A&M University/Texas A&M Transportation Institute

Yong-Rak Kim
Professor
Associate Director, Center for Railway Research
Civil Engineering Department
Texas A&M University

A Report on Research Sponsored by

University Transportation Center for Railway Safety (UTCRS)

Texas A&M University

September 30, 2024

Technical Report Documentation Page

1. Report No. UTCRS-TAMU-I1CY23	2. Government Accession No.	3. Recipient's Catalog No.
4. Title and Subtitle Enhancing the TAMU Model for Predicting Buckling in Rails		5. Report Date September 30, 2024
		6. Performing Organization Code UTCRS-TAMU
7. Author(s) D.H. Allen, T.-M. Liu, and Y.-R. Kim		8. Performing Organization Report No. CRR-2024-02
9. Performing Organization Name and Address University Transportation Center for Railway Safety (UTCRS) Texas A&M Transportation Institute (TTI) Texas A&M University (TAMU) College Station, TX 77843		10. Work Unit No. (TRAIS)
		11. Contract or Grant No. 69A3552348340
12. Sponsoring Agency Name and Address U.S. Department of Transportation (USDOT) University Transportation Centers Program 1200 New Jersey Ave. SE Washington, DC, 20590		13. Type of Report and Period Covered Project Report June 1, 2023-August 31, 2024
		14. Sponsoring Agency Code USDOT UTC Program
15. Supplementary Notes Conducted in collaboration with MxV Rail		

16. Abstract

It is well-known that track buckling is one of the most commonplace causes of train derailments. Accordingly, with partial funding provided by our previous USDOT UTC and the Technology Transportation Center, Inc., we have begun developing a Beta-version track buckling model for deployment by U.S. Railroad Companies as a tool for predicting track buckling. A significant advancement over currently deployed track buckling models, our technology includes an open-source nonlinear finite element algorithm that is user-friendly. Briefly, our track buckling model accounts for the effects of the following on track buckling: both longitudinal and lateral track walk; rail neutral temperature (RNT); both lateral and longitudinal crosstieaggregate interfacial friction; track modulus; nonlinear track liftoff; and broken spikes. In addition, it is sufficiently robust to be capable of accounting for additional environmental causes to be described herein and in a companion proposal. Given these advanced capabilities, track engineers will be able to dramatically improve track safety. The report given herein is a draft of a paper to be submitted for publication in a refereed journal.

17. Key Words Construction, Maintenance, Civil Engineering, Railroad Tracks, Buckling	18. Distribution Statement This report is available for download from https://www.utrgv.edu/railwaysafety/research/infrastructure/index.htm		
19. Security Classification (of this report) None	20. Security Classification (of this page) None	21. No. of Pages 30	22. Price

Table of Contents

List of Figures

List of Tables

List of Abbreviations

FE	Finite Element
FEM	Finite Element Method
FRA	Federal Railroad Administration
RNT	Rail Neutral Temperature
USDOT	U.S. Department of Transportation
UTC	University Transportation Centers

Disclaimer

The report given herein is a draft of a paper to be submitted for publication in a refereed journal. The contents of this report reflect the views of the authors, who are responsible for the facts and the accuracy of the information presented herein. This document is disseminated under the sponsorship of the U.S. Department of Transportation's University Transportation Centers Program, in the interest of information exchange. The U.S. Government assumes no liability for the contents or use thereof.

Acknowledgments

The authors wish to acknowledge the University Transportation Center for Railway Safety (UTCRS) for funding this project under the USDOT UTC Program Grant No 69A3552348340. We acknowledge the input provided to this research by Dr. Stephen Wilk, research scientist at MxV Rail, Pueblo, CO.

Developing a Finite Element Model for Predicting Rail Buckling Induced by Initial Misalignments

T. Liu, V. Musu, D. H. Allen, S. Wilk

Abstract

Due to its complexity, rail buckling is a mathematically nonlinear phenomenon affected by a wide range of service conditions, including but not limited to field temperature, track geometry, tie-ballast interactions, material properties of the structural components, train-induced lift-off, and different types of boundary conditions. Although several research studies have focused on this issue, it is still challenging to model this problem efficiently while maintaining both simplicity and accuracy. This research team has developed a finite element (FE) computer code based on the Euler-Bernoulli beam theory (Euler, 1744) to account for all the above phenomena, thereby resulting in a Python-based FE program that only requires a few seconds of runtime to complete one buckling simulation.

Building on the previous work by (Musu, Allen, & Fry, 2024), this study extends the model's development by expanding the nonlinear solving algorithm, as well as modifying the tie-ballast interface resistance formulation, and restructuring the variational formulation of the governing differential equations.

The key focus of this research is to analyze how initial rail misalignments affect buckling. In addition, a nonlinear tie-ballast resistance formulation is applied within this model to represent single-tie push test (STPT) experimental outputs to provide more realistic results. Results herein show that, as misalignment increases, the critical rail buckling load decreases significantly, making it a crucial factor in the prediction of rail buckling.

Rail Structures, Buckling, Finite Element Method, Euler-Bernoulli Beam Theory, Geometrical Nonlinearity, Rail Misalignment, Single-Tie Push Test

1. Introduction

Rail buckling is a catastrophic event that can cause serious safety issues in the rail industry. According to studies (Federal Railroad Administration, 2024), around 11% of the total railroad

accidents within the last three years (2021~2023) could be related to buckling. These accidents can result in billions of dollars lost and even lead to human casualties. However, today, there are still no clear guidelines for protecting against rail buckling.

Figure 1: *Photograph showing thermally induced buckling of a railway (reprinted with permission from ABproTWE, CC BY-SA 3.0, via Wikimedia Commons)*

Rail buckling is a type of structural instability oftentimes induced by thermal effects. Railroad engineers note that buckling usually happens in summer and during the day when the ambient temperature is high. However, field observations also show that rail misalignments (track-walk), broken fasteners (spikes), tie-ballast resistance performance, and other imperfections could also affect rail buckling. Even though modern commercial finite element software can solve this problem, the expense, the training needed, and the necessary computation time obviate deployment of commercially available codes in the field. Accordingly, an efficient method, which nonetheless includes a minimum level of complexity, needs to be developed to prevent rail buckling.

The body of literature on this subject is extensive. In the 18th century, the first concise beam-bending model was reported (Euler, 1744). Two centuries later, Timoshenko applied this procedure to predict deformations of railroad structures (Timoshenko, 1915, 1927). Though not

specific to rails, the vertical deformation of a beam on an elastic foundation has also been investigated (Oden, 1967).

More recently, Kerr formulated a detailed rail-response-predicting model utilizing beam theory (Kerr, 1974; Kerr et al., 1976), and soon thereafter, the rail buckling problem started to gain more attention. A finite element model deploying the previously mentioned formulation was used to analyze the relation between buckling temperature, initial lateral imperfections, and elastic-plastic type ballast resistance (Tvergaard and Needleman, 1981). Lift-off problems and wheel-track interaction have also been analyzed (Dong et al., 1994). A series of experimental and numerical studies on the stability of continuously welded rail (CWR) and thermal buckling made significant progress in this field, which led to the development of Fourier analysis models that incorporate vehicle loads or operate without them (Kish et al., 1982, 1985; Kish and Samavedam, 1991, 2013). Research has also shown that vertical displacements can also affect rail buckling, suggesting that describing the problem as 2D may be an oversimplification (Lim et al., 2003). Several researchers have also conducted post-buckling analyses of rails (Li and Batra, 2007; Yang and Bradford, 2016).

As it is gaining popularity, commercial finite element software is used to analyze rail buckling problems (Pucillo, 2016; Miri et al., 2021). However, some shortcomings of current solving procedures, such as solving an overly simplified boundary value problem, extended runtime, operating difficulty, and limited flexibility, must be resolved to provide practical and prompt support to railroad safety inspectors.

With these thoughts in mind, a finite element computational algorithm is developed within this research as a means of providing readily accessible yet accurate predictions of rail buckling as a function of a wide range of environmental factors. The current research extends the previous work done by Musu et al. (2024), which emphasized lift-off effects. By modifying the nonlinear solving procedure, the updated model has significantly improved efficiency. Also, additional causal factors are deployed within the model, including initial rail misalignment and nonlinear tie-ballast resistance effects.

2. Model Development

This section will briefly describe the assumptions deployed in the development of the model used in this research. Further details of the derivation are available in (Musu, 2023).

2.1. Overview of The Track Structure

As illustrated in Fig. 2, the track is affixed to the crossties using fasteners (spikes). The ballast, composed of crushed stone aggregate, is deposited on the rail bed beneath the ties, which are typically embedded within it. Note that the coordinate axes x, y, and z correspond to the axial, lateral, and vertical directions relative to the direction of travel.

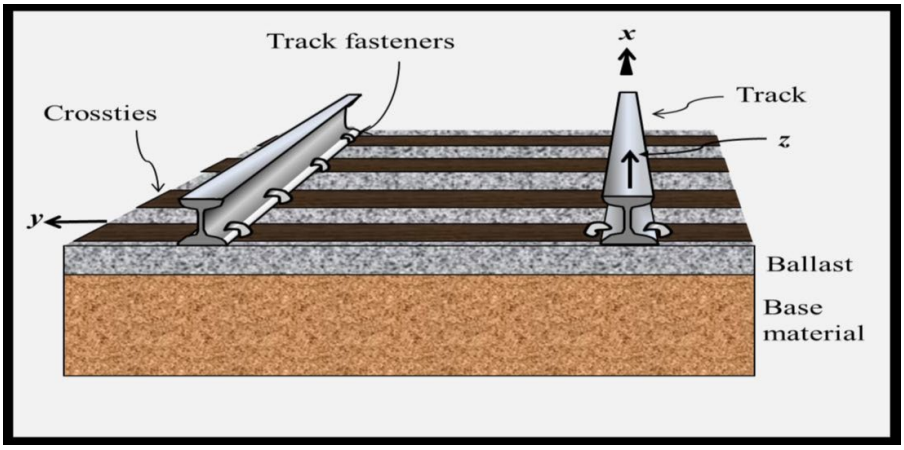

Figure 2: Generic rail with right-handed coordinate system as shown

2.2. Effects on the Track

The ties attached to the track provide some resistance to help prevent the track from deforming. The tie-ballast interaction provides resistance, and research has shown that this can be a highly nonlinear effect (Samavedam et al., 1995).

For lateral resistance F_y, this research has deployed the results of single-tie push tests (STPT) (Wilk, 2024). STPTs are experiments that apply a lateral load to a single tie embedded within the track structure to measure the force-displacement relationship, as depicted in Fig. 3.

Although the tie is disconnected from the original track, it is still embedded in the ballast, implying that the resistance measured is caused strictly by the tie-ballast interaction. In general, the relationship between the resistance and lateral displacements v can be expressed by a nonlinear curve with a stiff initial slope, which converges to a constant value F_{cr} as the lateral displacement increases, as shown in Fig. 4. For curve-fitting purposes, the resistance curve in the model is expressed as a piecewise continuous polynomial, as shown in Eq. 1.

Figure 3: Photograph showing the operation of a single-tie push test experiment conducted by MxV Rail, Pueblo, CO

$$F_y(v) = \begin{cases} \frac{F_{cr}}{v_{cr}} |v| \cdot sgn(-v) & \text{, if } |v| \le (1-\gamma)v_{cr} \\ \frac{-F_{cr}}{4\gamma}\left[\frac{1}{{v_{cr}}^2}|v|^2 - \frac{2(1+\gamma)}{v_{cr}}|v| + (1-\gamma)^2\right] \cdot sgn(-v) & \text{, if } (1-\gamma)v_{cr} < |v| < (1+\gamma)v_{cr} \\ F_{cr} \cdot sgn(-v) & \text{, if } (1+\gamma)v_{cr} \le |v| \end{cases} \quad (1)$$

where v_{cr} is the critical displacement, and γ is an artificial parameter that controls the smoothness of the slope transition. In addition, the initial slope of the resistance curve, k_y, is defined as:

$$k_y = \frac{F_{cr}}{v_{cr}} \quad (2)$$

Even though research showed that the relationship between axial resistance, F_x, and axial displacement, u, is also nonlinear (Tvergaard and Needleman, 1981; Nobakht et al., 2022), the precise mechanism for this type of load has not yet been determined. For simplicity, the axial resistance deployed herein is assumed to be linear in the axial displacement, as shown below:

$$F_x(u) = -k_x\, u \quad (3)$$

where k_x is assumed to be a constant.

Fasteners are used to connect tracks and ties and can provide rotational resistance to prevent the rail from bending, as shown in Fig. 5.

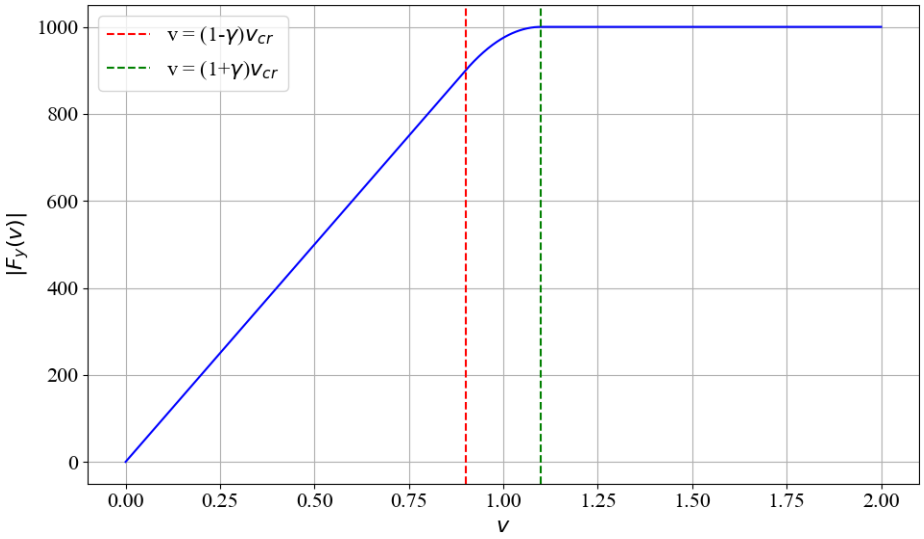

Figure 4: Demonstration of the lateral tie-ballast resistance $|F_y(v)|$ vs. lateral displacements v curve, for $F_{cr} = 1000$, $v_{cr} = 1$, $\gamma = 0.1$

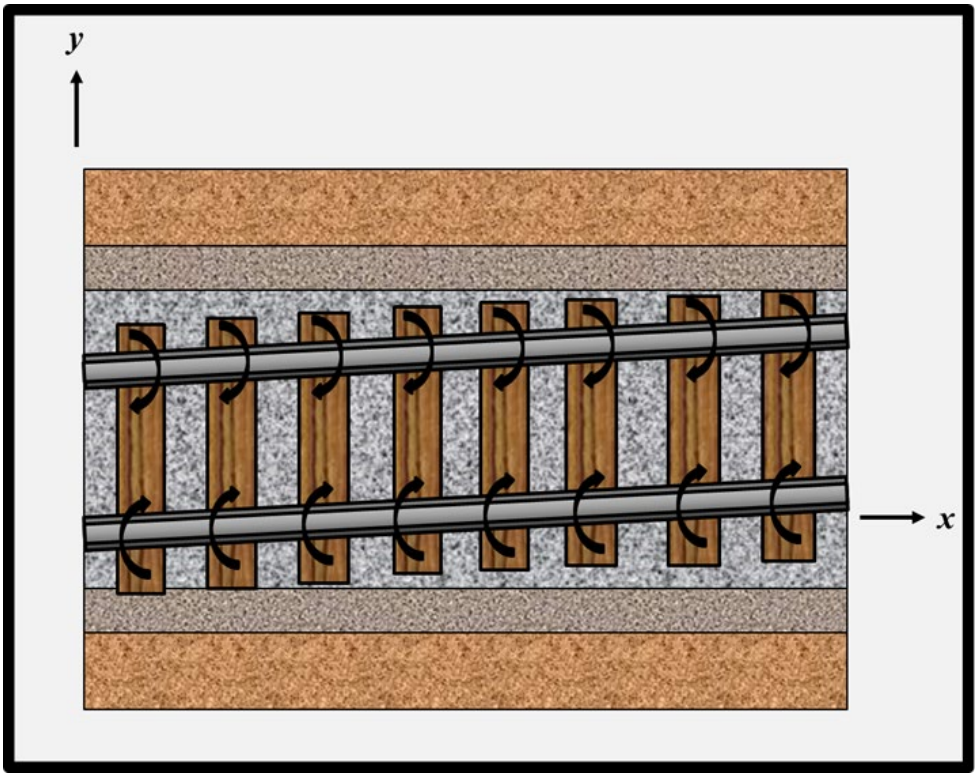

Figure 5: Demonstration of the rotational resistance induced by fasteners and ties

Similar to the axial resistance, the precise amount of rotational resistance that is provided by the fastener as a function of the rotation angle, θ_z, is still unclear. In addition, the relationship may also be nonlinear and strongly dependent on the fastener type (Samavedam et al., 1993). In the current paper, it is assumed that the rotational stiffness, S, is a constant as shown in Eq. 4.

$$m_z(\theta_z) = -S\theta_z \tag{4}$$

Contrary to the x and y directions, friction is assumed to be negligible in the z direction. Nonetheless, the vertical support of the foundation (ballast), r_z, is assumed to be a linear function of the vertical displacements, w, and can be expressed as:

$$r_z(w) = -k_z w \tag{5}$$

where the track modulus, k_z, is assumed to be a constant and can be acquired from experimental data (Oden, 1967).

Rail buckling is usually induced by thermal effects, including high ambient temperature, direct sunlight, and/or frictional heating caused by vehicle operation. Thus, the thermal stresses caused by thermal expansion must be taken into consideration. A linear thermoelastic constitutive equation is deployed within this model, given by:

$$\sigma_{xx} = E(\varepsilon_{xx} - \alpha \Delta T) \tag{6}$$

where E is the Young's modulus, ε_{xx} is the axial strain, α is the coefficient of thermal expansion, and ΔT is the current temperature difference compared to the rail neutral temperature (RNT), implying that at RNT there will be no thermal stress applied to the system.

Finally, other sources of loads or moments applied to the track, such as vehicle loads, could be described as distributed loads or concentrated point loads applied to the beam. The means by which these additional external loadings could affect rail buckling will be discussed in later sections.

2.3. Boundary Value Problem

As the rail is slender, and the axial dimension is much greater than the lateral and vertical dimensions, we will apply the Euler-Bernoulli assumption to our model, meaning that cross-sections of the track always remain planar and normal to the centroidal axis. Based on the assumption, we have the following results: (1) transverse normal stress components σ_{yy} and σ_{zz}, as shown in Fig. 6, can be neglected compared to axial normal stress σ_{xx}; (2) the displacement fields are a function of x only (Euler, 1744; Allen and Haisler, 1985; Grissom and Kerr, 2006).

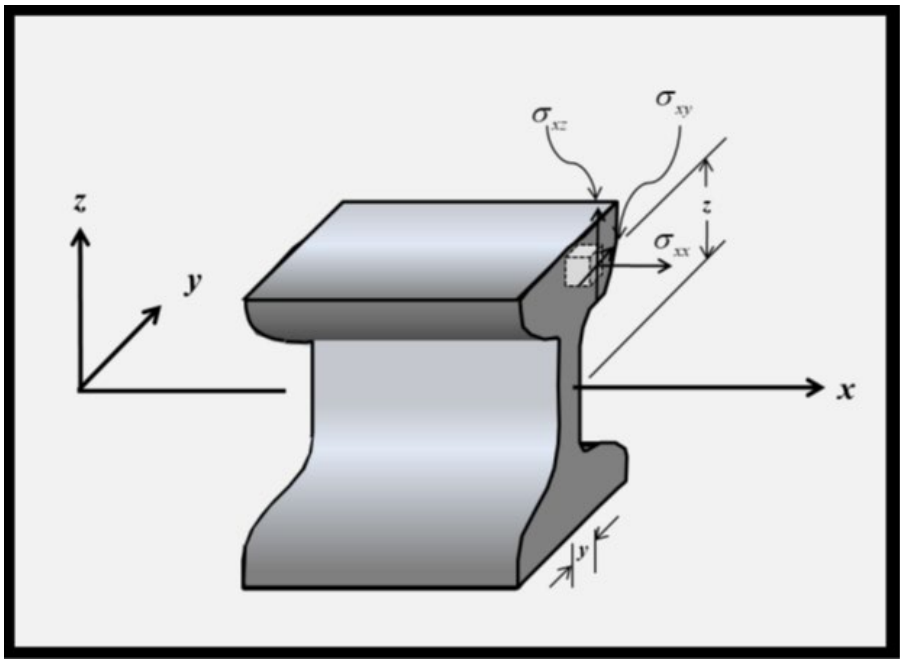

Figure 6: Demonstration of the normal stress components of an infinitesimal element within the rail

According to field observations, rotation about the x-axis (torsion) is a relatively minor issue in rail buckling. Thus, a 3-D model with 5 degrees of freedom, excluding torsion, is developed herein. After applying Euler-Bernoulli beam theory to our problem, we can replace the effect of stress components σ_{xx}, σ_{yy}, σ_{zz}, σ_{xy}, and σ_{xz}, with resultant loads P, V_y, V_z and moments M_y, M_z. The resulting free-body diagrams are shown in Fig. 7, where u_0, v_0, w_0 are the displacements at the centroid in the x, y, z direction, p_x, p_y, p_z are the distributive loads applied to the element, and r_z is the ballast support in the vertical direction, explained in the previous section. Note that the x-y plane is depicted as a deformed body, while the x-z plane remains undeformed. The reason is that, due to the difference between the moments of inertia I_{yy} and I_{zz}, buckling in the x-y plane happens much more frequently, and the geometric nonlinearity of this plane is also the main focus of this research. Even though vertical buckling can happen, but only when lateral displacements are constrained, it is rare. Thus, large vertical deformations are generally negligible and will not be considered in this research.

Regarding axial strain, the formulation when considering large deformations is given by:

$$\varepsilon_{xx} = \frac{du}{dx} + \frac{1}{2}\left[\left(\frac{du}{dx}\right)^2 + \left(\frac{dv}{dx}\right)^2 + \left(\frac{dw}{dx}\right)^2\right] \tag{7}$$

As we know, lateral displacements are much more significant than the other two directions for the lateral bucking problem, $\frac{1}{2}\left(\frac{dv}{dx}\right)^2$ will be the only second-order term that needs to be taken into consideration (Tvergaard and Needleman, 1981; Grissom and Kerr, 2006), so that the final strain-displacement relationship utilized herein is therefore given by:

$$\varepsilon_{xx} = \frac{du}{x} + \frac{1}{2}\left(\frac{dv}{dx}\right)^2 \tag{8}$$

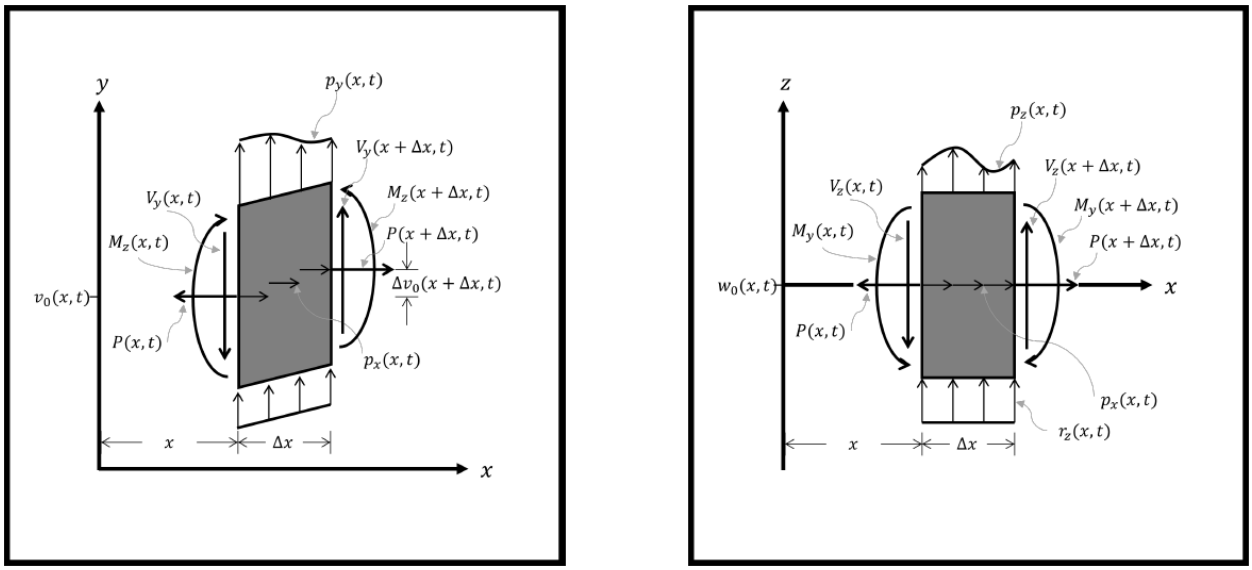

Figure 7: Resultant forces and moments applied to a differential element within the rail in the (a) x-y plane, and (b) x-z plane

Finally, it is assumed that the rotational angles are small and can be described by:

$$\theta_y \cong tan(\theta_y) = -\lim_{\Delta x \to 0} \frac{\Delta w_0}{\Delta x} = -\frac{dw_0}{dx} \tag{9a}$$

$$\theta_z \cong tan(\theta_z) = \lim_{\Delta x \to 0} \frac{\Delta v_0}{\Delta x} = \frac{dv_0}{dx} \tag{9b}$$

We assume that the problem is quasi-static, and the only independent variable will be x. Applying the equilibrium equations and utilizing Eq. 6 to 9 while considering tie-ballast resistances and fastener resistances as external point loads and moments, we have constructed a well-posed initial quasi-static boundary value problem, as shown in Table 1:

Table 1: Initial boundary value problem for predicting rail response

1. Independent Variables: x
2. Known inputs: Load: $p_x = p_x(x),\ p_y = p_y(x),\ p_z = p_z(x), \qquad 0 < x < L$

   Temperature change: ΔT = known

   Geometry: $A, I_{yy}, I_{zz}, L, y, z$

   Material Properties: α, E, k_z
3. Dependent variables: $u_0 = u_0(x),\ v_0 = v_0(x),\ w_0 = w_0(x),\ P = P(x),$

   $V_y = V_y(x),\ V_z = V_z(x),\ M_y = M_y(x),\ M_z = M_z(x),\ \sigma_{xx} = \sigma_{xx}(x),$
4. Field equations:

$$\frac{dP}{dx} = -p_x \tag{8a}$$

$$\frac{dV_y}{dx} = -p_y \tag{8b}$$

$$\frac{dV_z}{dx} = -p_z + k_z w_0 \tag{8c}$$

$$\frac{dM_y}{dx} = V_z \tag{8d}$$

$$\frac{dM_z}{dx} = -V_y + P\frac{dv_0}{dx} \tag{8e}$$

$$\frac{du_0}{dx} = \frac{\left(P + P^T\right)}{EA} - \frac{1}{2}\left(\frac{dv_0}{dx}\right)^2 \tag{8f}$$

$$\frac{d^2v_0}{dx^2} = \frac{M_z}{EI_{zz}} \tag{8g}$$

$$\frac{d^2w_0}{dx^2} = -\frac{M_y}{EI_{yy}} \tag{8h}$$

$$\sigma_{xx} = \frac{P}{A} - \frac{M_z y}{I_{zz}} + \frac{M_y z}{I_{yy}} \tag{8i}$$

$$P^T = E\,A\,\alpha\,\Delta\,T \tag{8j}$$

There are 9 equations and 1 additional auxiliary equation (the thermoelastic constitutive relation) for solving the listed 9 dependent variables. Even though the problem is well-posed, the highly coupled relations make it nonetheless rather difficult to obtain analytic solutions without making certain simplifying assumptions. As a result, in order to avoid deploying these necessarily debilitating assumptions, a numerical solving procedure utilizing FEM is proposed herein.

2.4. Finite Element Method

To solve the coupled equations in Table 1, we apply the principle of virtual work to Eq. 8a, 8b, and 8c:

$$\int_0^L \left[\frac{dP}{dx} + p_x\right] \delta u \, dx + \int_0^L \left[\frac{dV_y}{dx} + p_y\right] \delta v \, dx + \int_0^L \left[\frac{dV_z}{dx} + P_z - k_z w\right] \delta w \, dx = 0 \tag{10}$$

Note that the "0 "subscripts of u, v, and w are dropped to make the expression more concise. Through a series of integration by parts and equation substitution, we can come up with the final weak form of our problem:

$$\begin{aligned} &\int_0^L E\,A \frac{du}{dx} \delta\left(\frac{du}{dx}\right) dx + \int_0^L E\,I_{zz} \frac{d^2v}{dx^2} \delta\left(\frac{d^2v}{dx^2}\right) dx + \int_0^L E\,I_{yy} \frac{d^2w}{dx^2} \delta\left(\frac{d^2w}{dx^2}\right) dx \\ -(-&\int_0^L E\,A \frac{du}{dx}\frac{dv}{dx}\,\delta\left(\frac{dv}{dx}\right) dx - \int_0^L \frac{EA}{2}\left(\frac{dv}{dx}\right)^2 \delta\left(\frac{du}{dx}\right) dx - \int_0^L \frac{EA}{2}\left(\frac{dv}{dx}\right)^3 \delta\left(\frac{dv}{dx}\right) dx \\ &- \int_0^L k_z\, w\delta w \, dx + \int_0^L p_x\ \delta u \, dx + \int_0^L p_y\ \delta v \, dx + \int_0^L p_z\ \delta w \, dx \\ &+ \int_0^L P^T\ \delta\left(\frac{du}{dx}\right) dx + \int_0^L P^T\ \frac{dv}{dx}\ \delta\left(\frac{dv}{dx}\right) dx \\ &+[P\ \delta u]_0^L + [V_y\ \delta v]_0^L + [V_z\ \delta w]_0^L + [M_y \delta(\theta_y)]_0^L + [M_z \delta(\theta_z)]_0^L) = 0 \end{aligned} \tag{11}$$

As we can see, there are several different sources of nonlinearity such as: geometric nonlinearity (term 4 and term 6), nonlinearity caused by strain-displacement relationship (term 5, term 6). In addition, though not shown in the weak formulation, nonlinearities caused by point loads and moments, such as tie-ballast resistances, will also be included in this model, entering the system by specifying realistic boundary conditions.

To solve the weak form with the finite element method, we employ Hermite shape functions of cubic order (Allen and Haisler, 1985):

Substituting into the weak formulation, we have:

$$\sum_{i=1}^{10} (I_i^e - F_i^e)\ \delta q_i = 0 \tag{12a}$$

where:

$$I_i^e = \int_0^{L^e} [\, EA \frac{d}{dx}\left(\sum_{m=1}^{10} \xi_m\, q_m\right)\frac{d\xi_i}{dx} + EI_{zz}\frac{d^2}{dx^2}\left(\sum_{m=1}^{10} \eta_m\, q_m\right)\frac{d^2\eta_i}{dx^2} + EI_{yy}\frac{d^2}{dx^2}\left(\sum_{m=1}^{10} \zeta_m\, q_m\right)\frac{d^2\zeta_i}{dx^2}]dx \tag{12b}$$

$$F_i^e = F_{\text{Geo},i}^e + F_{\text{LS},i}^e + F_{\text{LS,Geo},i}^e + F_{\text{Bal},i}^e + F_{\text{Dis},i}^e + F_{\text{T},i}^e \tag{12c}$$

The vector F_i^e includes the applied external forces, thermal loads, and ballast vertical resistance. Additionally, it incorporates the nonlinear effect terms, which are defined as pseudo-forces (Haisler et al., 1972). Each term is defined below:

$$F_{\text{Geo},i}^e = -\int_0^{L^e}\left[EA\frac{d}{dx}\left(\sum_{m=1}^{10}\xi_m\, q_m\right)\frac{d}{dx}\left(\sum_{n=1}^{10}\eta_n\, q_n\right)\frac{d\eta_i}{dx}\right]dx \tag{13}$$

$$F_{\text{LS},i}^e = -\int_0^{L^e}\left[\frac{EA}{2}\frac{d}{dx}\left(\sum_{m=1}^{10}\eta_m\, q_m\right)\frac{d}{dx}\left(\sum_{n=1}^{10}\eta_n\, q_n\right)\frac{d\xi_i}{dx}\right]dx$$

$$F_{\text{LS,Geo},i}^e = -\int_0^{L^e}\left[\frac{EA}{2}\frac{d}{dx}\left(\sum_{m=1}^{10}\eta_m\, q_m\right)\frac{d}{dx}\left(\sum_{n=1}^{10}\eta_n\, q_n\right)\frac{d}{dx}\left(\sum_{r=1}^{10}\eta_r\, q_r\right)\frac{d\eta_i}{dx}\right]dx$$

$$F_{\text{Bal},i}^e = -\int_0^{L^e}\left[k_z\left(\sum_{m=1}^{10}\zeta_m\, q_m\right)\zeta_i\right]dx$$

$$F_{\text{Dis},i}^e = \int_0^{L^e}\left[p_x\xi_i + p_y\eta_i + p_z\zeta_i\right]dx$$

$$F_{\text{T},i}^e = \int_0^{L^e}\left[P^T\frac{d\xi_i}{dx} + P^T\frac{d}{dx}\left(\sum_{m=1}^{10}\eta_m\, q_m\right)\frac{d\eta_i}{dx}\right]dx$$

Where F_{Geo} represents terms caused by geometric nonlinearity, F_{LS} represents terms caused by large strain effects in the axial direction, $F_{LS,Geo}$ represents terms caused by geometric nonlinearity when considering large strain effects, and F_{Bal}, F_{Dis}, and F_T represent terms caused by ballast resistance, distributive loads, and thermal effects, respectively.

Note that we have already dropped the resultant force and moment terms at the boundary as they will cancel out each other when assembling from local form into global form. Since δq_i should be mutually linear independent, and Eq. 12 is always true, we obtain a set of 10 equations:

$$I_i^e = F_i^e, \text{ for } i = 1 \text{ to } 10 \tag{14}$$

To solve this system, we first apply a Taylor expansion. We know that I_i^e is a function of the current displacement values q_i. If we expand against $I_i^e(q_j)$:

$$I_i^e(q_j + \Delta q_j) = I_i^e(q_j) + \frac{\partial I_i^e}{\partial q_j}\Delta q_j + \frac{1}{2}\frac{\partial^2 I_i^e}{\partial {q_j}^2}(\Delta q_j)^2 + H.O.T \tag{15}$$

As the displacement increments between different time-steps are relatively small, we can neglect higher-order terms. Only considering only zero and first-order terms, we obtain the following:

$$K_{ij}^e \Delta q_j = I_i^e(q_j + \Delta q_j) - I_i^e(q_j) \tag{16a}$$

where the Jacobian matrix of I_i^e, or so-called the stiffness matrix, is defined by:

$$K_{ij}^e = \frac{\partial I_i^e}{\partial q_j} \tag{16b}$$

Regarding Eq. 14, we obtain the following final form of the incremental equilibrium equations:

$$K_{ij}^e \Delta q_j = \Delta F_i^e \tag{17a}$$

$$\Delta F_i^e = F_i^e(q_j + \Delta q_j) - F_i^e(q_j) \tag{17b}$$

Utilizing the standard FE assembly method, the local stiffness matrices and force vectors are assembled into the global form to model the entire rail section. By applying axial loads (due to force or temperature change), the displacements can be obtained by Eq. 17a.

2.5. Accounting for Nonlinearity

In order to accurately account for the nonlinearities within ΔF_i, an increment of loading, we divide the entire loading procedure into several time-steps. At each time-step we apply the same amount of load or temperature change, and each step is assumed to be quasi-static. Displacement values applied to the force vector need to be updated within each step, and for more accurate results, iterative methods, such as Newton's method are deployed within this model. The concept of Newton's method is to use results of previous iterations to obtain an improved estimate for the next iteration, and the procedure is terminated when it satisfies a convergence criterion related to the residual $R(\Delta q_j^m)$ at iteration m, defined as follows:

$$R(\Delta q_j^m) = ||\Delta F_i(q_j + \Delta q_j^m) - K_{ij}\Delta q_j^m|| \tag{18}$$

which is the Euclidean norm of the difference between the two terms in Eq. 17a. Using Taylor's Formula to expand $R(\Delta q_j^m)$ against q_j^m while neglecting higher order terms results in:

$$R\left(\Delta q_j^m\right) = -\frac{\partial R\left(\Delta q_j^m\right)}{\partial \Delta q_j^m}\left(\Delta q_j^{m+1} - \Delta q_j^m\right) \tag{19}$$

We then solve Eq. 19 repeatedly until $R\left(\Delta q_j^m\right)$ reaches a value smaller than the convergence criterion. The convergence criterion is a constant decided a priori and should be a small number, close to 0. It is set to 6×10^{-6} in this research. Once this condition is satisfied, the displacement change between iteration $m+1$ and m is negligible, and convergence at the time-step is reached, and the new displacement vector $\Delta q_{j,new}$ can be obtained by the displacement vector at the previous step $\Delta q_{j,old}$, and the converged displacement change vector Δq_j^m:

$$\Delta q_{j,new} = \Delta q_{j,old} + \Delta q_j^m \tag{20}$$

In practice, calculating the Jacobian of the residual $\frac{\partial R\left(\Delta q_j^m\right)}{\partial \Delta q_j^m}$ is time-consuming and non-efficient. Thus, the Krylov subspace method is applied (Knoll and Keyes, 2004), where it utilizes the Generalized Minimal RESidual method (GMRES) (Saad and Schultz, 1986) approximate the Jacobian matrix with sub-iterations. The Newton-Krylov method has proven to be a highly efficient nonlinear system-solving procedure and has already been included in the current SciPy Module (Virtanen et al., 2020), this research utilizes this well-known function to solve the demonstrated problem.

2.6. Force-Control Algorithm

Either mechanical or thermal loads are applied to model rail buckling with the force-control algorithm. The corresponding load vs. displacement curve can be found by tracking the displacements at each load step, as shown in Fig. 8.

As the applied load value increases, the slope of the curve suddenly decreases, a process known as softening. For most cases, the displacement path can experience snap-through at the first unstable point as the load has reached its local maximum. In other cases, the curve could stiffen again, a process called progressive buckling, and does not have a significant unstable trend. Some researchers have shown that the value of the lateral tie-ballast resistance could cause the difference between these two cases (Samavedam et al., 1993; Kish and Samavedam, 2013). In this research, we define the point where the slope of the load vs. displacement curve becomes 0 as the buckling point and the corresponding load as the buckling load. The algorithm herein has been verified for several analytic solutions (Musu et al., 2020).

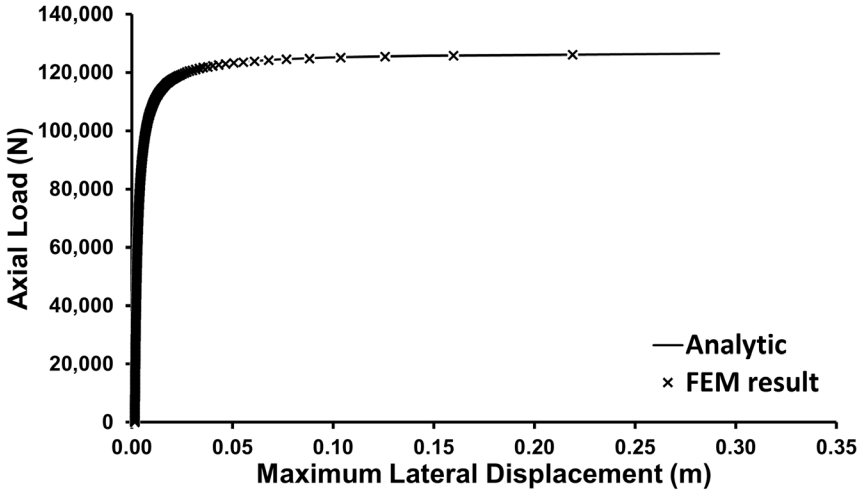

Figure 8: Demonstration of the axial load vs. maximum lateral displacement curve for a beam buckling problem while using load control

3. Results

This section utilizes the finite element model developed before to perform several rail buckling sensitivity studies. A number of different factors can affect the buckling load, including material properties, rail geometry, track modulus, fastener stiffness, tie-ballast resistance, and others. The main focus of this study will be on both the effect of tie-ballast lateral resistance and the shape of initial misalignments.

Buckling simulations are conducted on a 20-meter-long rail section, and the tie spacing is set at 0.5 meters. Both ends of the rail are assumed to be fixed, as no displacements or rotations are allowed. To show realistic buckling results, the geometry parameters are chosen based on the AREMA 115 RE rail head section, including the moment of inertia in both directions and the rail's cross-section area, and the material properties of steel are estimated based on industry specifications (Nippon Steel Corporation, 2020). Note that there are 2 aligned rails in the system, so geometric parameter values such as the cross-section area need to be multiplied by 2 before applying the model. All general input parameters are listed in Table 2.

Table 2: Rail and track parameters used in the sensitivity study

Rail Properties	Values	Units
Rail Length, L	20	*meter*
Tie-Spacing,	0.5	*meter*
Cross-Section, $2A$	1.45E-02	$meter^2$
Moment of Inertia, $2I_{yy}$	5.50E-05	$meter^4$
Moment of Inertia, $2I_{zz}$	9.00E-06	$meter^4$
Youngś Modulus, E	2.00E+11	*Pa*
Thermal Expansion Coefficient, α	1.05E-05	$1/°c$
Track Modulus, k_z	5.00E+08	*Pa*
Rotational Stiffness, S	2.25E+05	$N \cdot meter$

Initial geometric imperfections in the x-y plane should also be considered in the following cases, as secondary moments will be 0 if the rail is perfectly aligned. The initial imperfection shape can be described by a piecewise function, as shown in Eq. 21:

$$v(x) = \begin{cases} 0 & \text{, if } x < \frac{L}{2} - \frac{w}{2} \\ 16\frac{d}{w^4}\left(x - \frac{L}{2}\right)^4 - 8\frac{d}{w^2} * \left(x - \frac{L}{2}\right)^2 + d & \text{, if } \frac{L}{2} - \frac{w}{2} \leqq x \leqq \frac{L}{2} + \frac{w}{2} \\ 0 & \text{, if } x < \frac{L}{2} + \frac{w}{2} \end{cases} \quad (21)$$

where d is the initial displacement amplitude, and w is the width, as shown in Fig. 9. These two parameters are also the focus of this research.

In addition, it should be noted that even though the large strain formulation shown in Eq. 7 is included in the model, it is not utilized in the results shown in this research. The reason is that the gradient of the lateral displacement along the rail is still negligible, and adding the high-order terms does not significantly change the results. However, the terms could be critical in post-buckling analysis and need further verification.

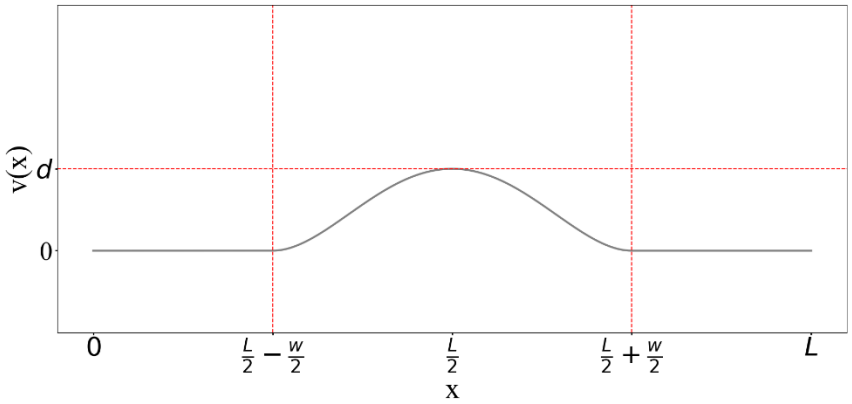

Figure 9: Demonstration of the rail geometry in the x-y plane when initial imperfections are applied (the track system is depicted as a single curve)

3.1. Effects of Lateral Tie-Ballast Resistance

Lateral tie-ballast resistance provides significant constraints to the rail at the early loading stage. As demonstrated in Eq. 1 and 4, a piecewise continuous function is applied to the model, representing STPT results. The curve is a function of the critical lateral displacement v_{cr} and critical maximum resistance F_{cr}, which are both input parameters used in the model.

STPT experiments typically show critical displacement values around 0.005 meters (0.2 inches) and maximum resistance values around 10000 Newtons (2000 pound force) (Kish and Samavedam, 2013; Khatibi et al., 2017; Wilk, 2024; Wilk et al., 2024). However, the results strongly depend on ballast condition and crosstie types, thus the numbers decided herein are only for demonstration purposes.

A sensitivity study was conducted by changing STPT parameters as the initial misalignment shape remained the same, using $w = 10$ meters and $d = 0.05$ meters.

First, the critical lateral displacement value v_{cr} was set to 0.005 meters, and the critical lateral resistance value F_{cr} was modified to range from 5000 Newtons to 20000 Newtons. Results are shown in Fig. 10 and 11.

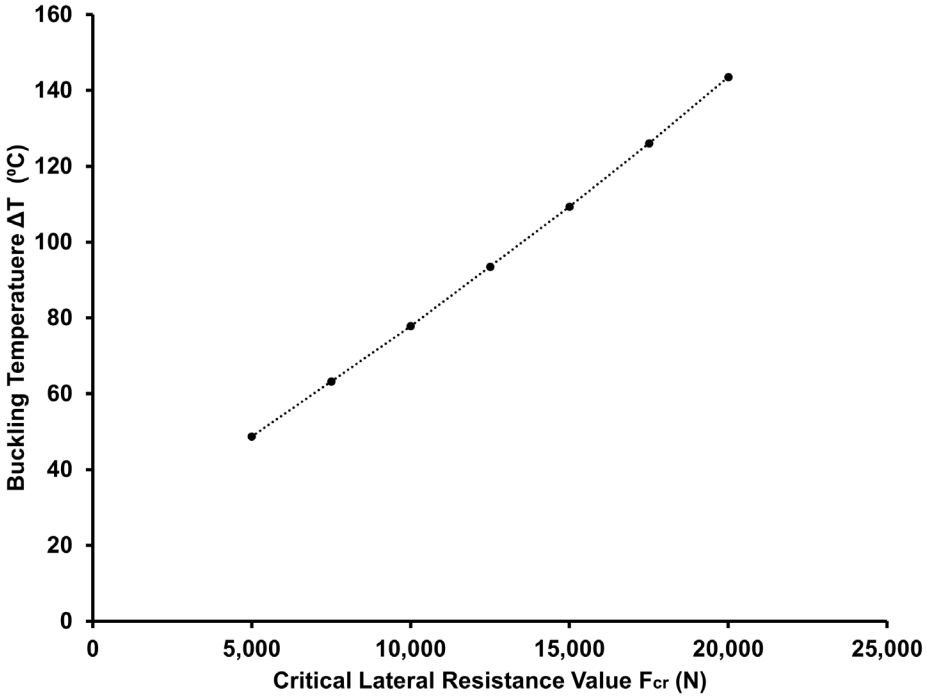

Figure 10: Predicted effect of maximum lateral ballast-tie resistance change on buckling temperature of a typical rail structure

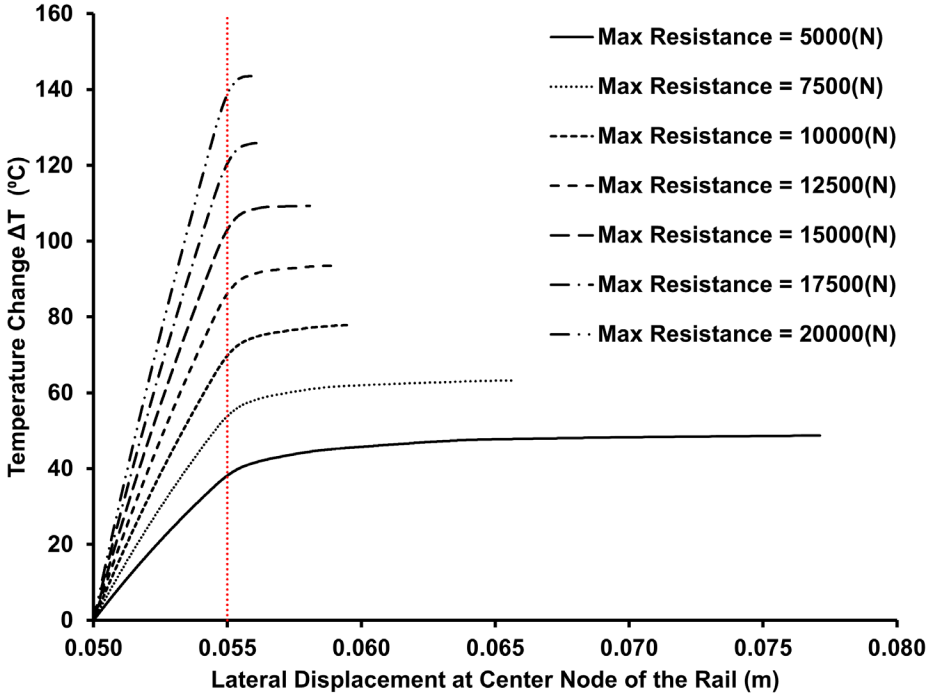

Figure 11: Maximum lateral displacement vs. applied temperature change before buckling with various maximum lateral ballast-tie resistance applied to a typical rail structure

Even though the slopes of the temperature-displacement curves are different for each case, the buckling process initiates at similar additional lateral displacements. Rapid lateral deformation started as soon as the additional lateral displacement value exceeded the critical displacement value v_{cr}, labeled as the red line in Fig. 11. This can be interpreted as the applied temperature difference being reasonably high. As soon as the effects of the tie-ballast lateral resistance fall off, the rail could buckle easily.

A critical displacement value sensitivity study was also conducted, as the initial misalignment shape remained the same, F_{cr} was set to 10000 Newtons, and v_{cr} ranged from 0.003 to 0.007 meters. As results are shown in Fig. 12 and 13, it could be noticed that the deformation rate has a significant difference between each case. However, even though the trend shows that the buckling temperature does decrease as v_{cr} decreases, the buckling temperature remains fairly close for these cases. In actual STPT experiments, the actual v_{cr} values could be difficult to capture accurately. However, the results represented herein have suggested that F_{cr} would be the more important factor affecting the buckling temperature and should be focused more on.

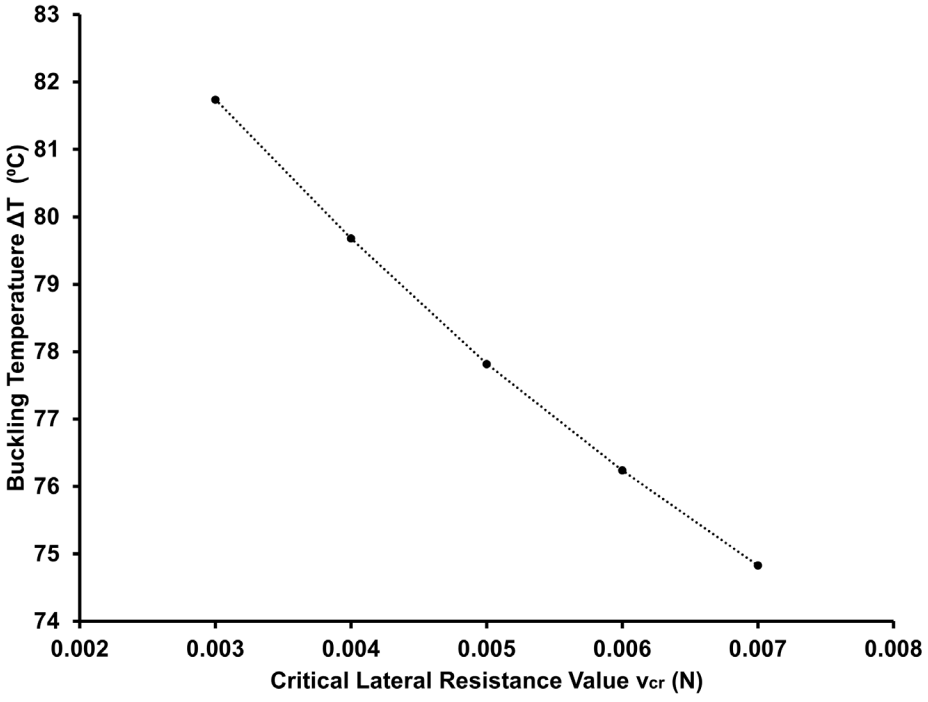

Figure 12: Predicted effect of maximum lateral ballast-tie resistance change on buckling temperature of a typical rail structure

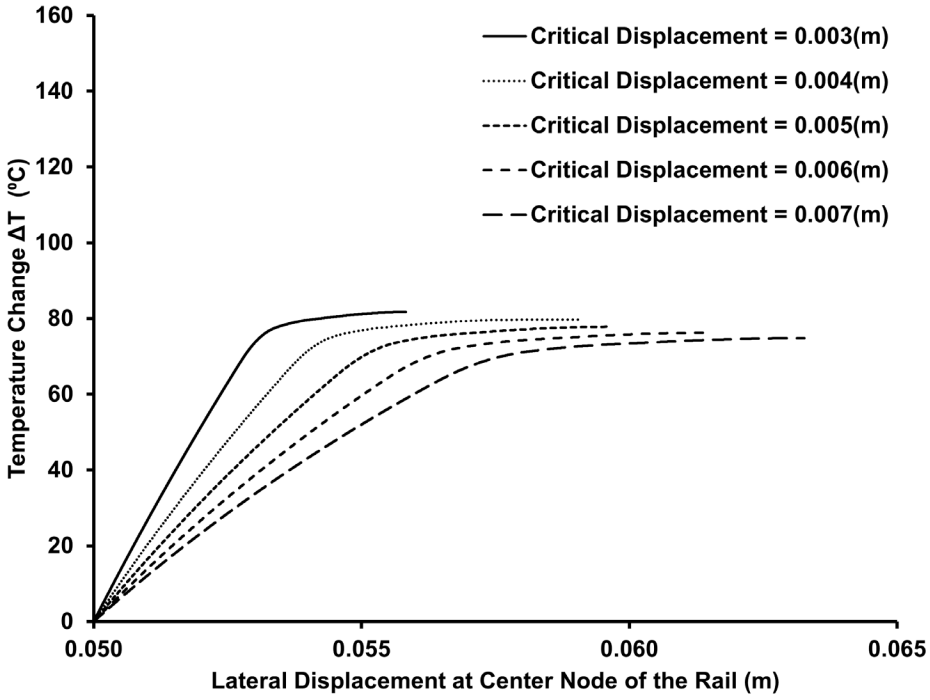

Figure 13: Maximum lateral displacement vs. applied temperature change before buckling with various maximum lateral ballast-tie resistance applied to a typical rail structure

3.2. Effects of Misalignment Amplitude

For misalignment problems, the lateral resistance parameters remain constant, with $v_{cr} = 0.005$ meters and $F_{cr} = 10000$ Newtons.

First, the amplitude of the initial imperfection curve is modified, ranging from 0.0125 meters to 0.1 meters, and results are shown in Fig. 14. It could be seen that the buckling temperature is highly sensitive to small initial misalignments and then converges to a smaller value as the amplitude increases. This suggests that in practice, even if the imperfection amplitude is small, it should still be treated with caution: while geometrically perfect aligned tracks could have extremely high buckling temperature, the buckling temperature experiences a 27% drop if the misalignment amplitude is doubled (from 0.0125(m) to 0.025(m)).

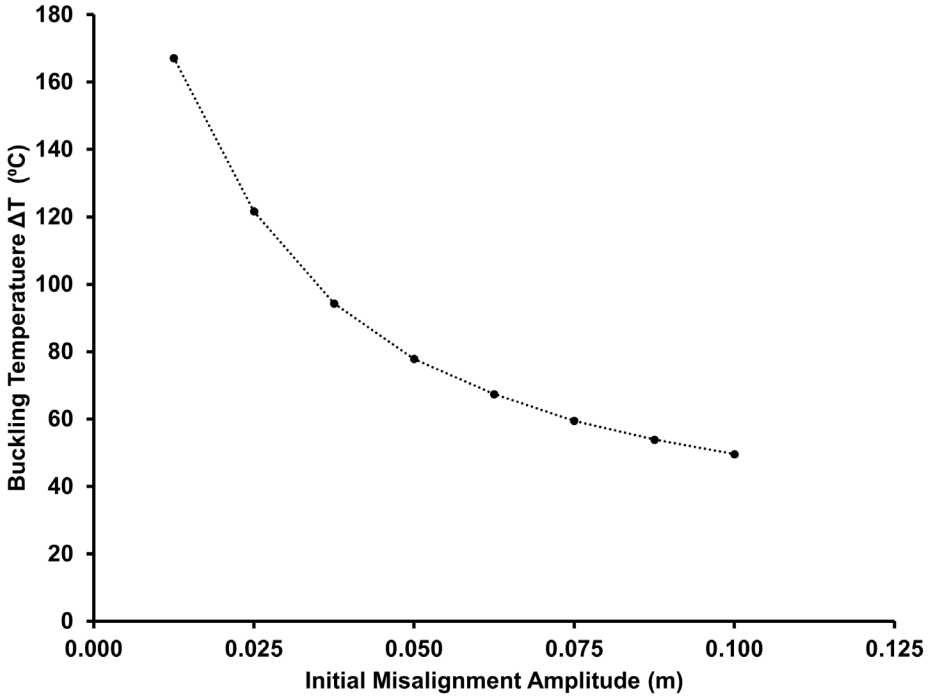

Figure 14: Predicted effect of maximum misalignment depth change on buckling temperature of a typical rail structure

3.3. Effects of Misalignment Width

The effects of the misalignment width are also considered. With the same lateral resistance parameters, the width changed from 3 to 10 meters. As shown in Fig. 15, the buckling temperature reaches a minimum when the misalignment width is around 6 meters. This could be because the imperfection shape is sharp at small widths, and the bending moment required to bend the rail would increase. However, as the width increases, the moment arm of the secondary moment effects decreases, and more axial stress is required to cause the same bending moment. As a result, the minimum buckling temperature happens in between.

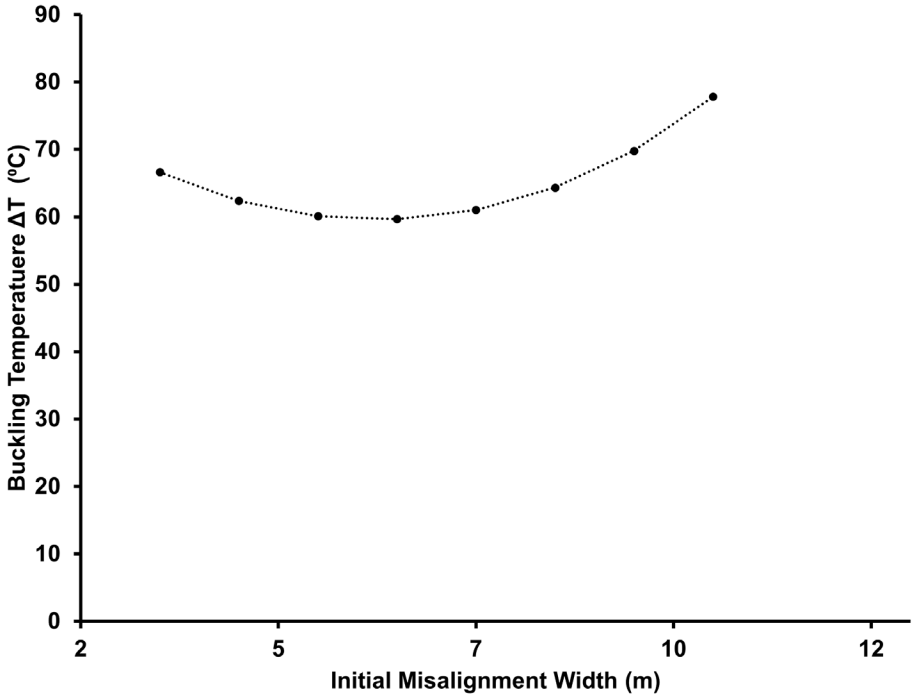

Figure 15: Predicted effect of maximum misalignment width change on buckling temperature of a typical rail structure

4. Conclusion

Herein, a robust nonlinear finite element model for predicting rail buckling is constructed. Sensitivity tests have been conducted so that STPT experiment results could be applied to the model. The results show that the critical resistance value plays a crucial role in rail buckling, and the relationship between these values behaves relatively linear. The effects of misalignment shape are also considered, and it is suggested that any small initial imperfections should be seriously considered to prevent derailments caused by rail buckling.

For future research, a displacement-control algorithm should be constructed based on the mathematical formulations depicted in this research and could be used for post-buckling analysis.

References

Allen, D.H., Haisler, W.E., 1985. Introduction to aerospace structural analysis.

Dong, R., Sankar, S., Dukkipati, R., 1994. A finite element model of railway track and its application to the wheel

flat problem. Proceedings of the Institution of Mechanical Engineers, Part F: Journal of Rail and Rapid Transit 208,61–72.

Euler, L., 1744. Methodus inveniendi Lineas Curvas.

Federal Railroad Administration, O.o.S.A., 2024. Train accidents and rates. URL: https://safetydata.fra.dot.gov/officeofSafety/publicsite/Query/TrainAccidentsFYCYWithRates.aspx.

Grissom, G.T., Kerr, A.D., 2006. Analysis of lateral track buckling using new frame-type equations. International

Journal of Mechanical Sciences 48, 21–32. URL: https://www.sciencedirect.com/science/article/pii/S0020740305002328, doi: https://doi.org/10.1016/j.ijmecsci.2005.09.006.

Haisler, W.E., Stricklin, J.A., Stebbins, F.J., 1972. Development and evaluation of solution procedures for geometrically nonlinear structural analysis. AIAA Journal 10, 264–272.

Kerr, A.D., 1974. The stress and stability analyses of railroad tracks .

Kerr, A.D., et al., 1976. Analysis of thermal track buckling in the lateral plane. Technical Report. United States. Federal Railroad Administration.

Khatibi, F., Esmaeili, M., Mohammadzadeh, S., 2017. Dem analysis of railway track lateral resistance. Soils and foundations 57, 587–602.

Kish, A., Samavedam, G., 1991. Dynamic buckling of continuous welded rail track: Theory, tests, and safety concepts. Transportation Research Record 1289, 23–38.

Kish, A., Samavedam, G., 2013. Track buckling prevention: theory, safety concepts, and applications. Report. John A.

Volpe National Transportation Systems Center (US).

Kish, A., Samavedam, G., Jeong, D.Y., 1982. Analysis of thermal buckling tests on US railroads. Report. United States. Federal Railroad Administration.

Kish, A., Samavedam, G., Jeong, D.Y., et al., 1985. Influence of vehicle induced loads on the lateral stability of CWR track. Technical Report. United States. Department of Transportation. Federal Railroad Administration.

Knoll, D.A., Keyes, D.E., 2004. Jacobian-free newton–krylov methods: a survey of approaches and applications. Journal of Computational Physics 193, 357–397.

Li, S.R., Batra, R., 2007. Thermal buckling and postbuckling of euler-bernoulli beams supported on nonlinear elastic foundations. AIAA journal 45, 712–720.

Lim, N.H., Park, N.H., Kang, Y.J., 2003. Stability of continuous welded rail track. Computers & Structures 81, 2219–2236.

Miri, A., Dhanasekar, M., Thambiratnam, D., Weston, B., Chan, T., 2021. Analysis of buckling failure in continuously welded railway tracks. Engineering Failure Analysis 119, 104989.

Musu, V., 2023. Development of a Model for the Prediction of the Effects of Multiple Distinct Modes of Nonlinearity on Rail Buckling. Thesis.

Musu, V., Allen, D.H., Fry, G.D., 2024. Computational model for predicting lift-off induced buckling in rail structures. Paper under review.

Nippon Steel Corporation, 2020. Rails. URL: https://www.nipponsteel.com/product/catalog_download/pdf/K003en.pdf. accessed: September 16, 2024.

Nobakht, S., Zakeri, J.A., Safizadeh, A., 2022. Investigation on longitudinal resistance of the ballasted railway track under vertical load. Construction and Building Materials 317, 126074. URL: https://www.sciencedirect.com/science/article/pii/S095006182103806X, doi: https://doi.org/10.1016/j.conbuildmat.2021.126074.

Oden, J.T., 1967. Mechanics of elastic structures.

Pucillo, G.P., 2016. Thermal buckling and post-buckling behaviour of continuous welded rail track. Vehicle System Dynamics 54, 1785–1807.

Saad, Y., Schultz, M.H., 1986. Gmres: A generalized minimal residual algorithm for solving nonsymmetric linear systems. SIAM Journal on Scientific and Statistical Computing 7, 856–869. URL: https://doi.org/10.1137/0907058, doi:10.1137/0907058, arXiv: https://doi.org/10.1137/0907058.

Samavedam, G., Kanaan, A., Pietrak, J., Kish, A., Sluz, A., et al., 1995. Wood tie track resistance charaterization and correlations study. Technical Report. United States. Department of Transportation. Federal Railroad Administration.

Samavedam, G., Kish, A., Purple, A., Schoengart, J., et al., 1993. Parametric Analysis and Safety Concepts of CWR Track Buckling. Technical Report. United States. Federal Railroad Administration.

Timoshenko, S., 1915. Strength of rails. Transactions of the Institute of Ways and Communications, St. Petersburg, Russia .

Timoshenko, S., 1927. Method of analysis of statical and dynamical stresses in rail .

Tvergaard, V., Needleman, A., 1981. On localized thermal track buckling. International Journal of Mechanical Sciences 23, 577–587.

Virtanen, P., Gommers, R., Oliphant, T.E., Haberland, M., Reddy, T., Cournapeau, D., Burovski, E., Peterson, P., Weckesser, W., Bright, J., van der Walt, S.J., Brett, M., Wilson, J., Millman,

K.J., Mayorov, N., Nelson, A.R.J., Jones, E., Kern, R., Larson, E., Carey, C.J., Polat, ˙I., Feng, Y., Moore, E.W., VanderPlas, J., Laxalde, D., Perktold, J., Cimrman, R., Henriksen, I., Quintero, E.A., Harris, C.R., Archibald, A.M., Ribeiro, A.H., Pedregosa, F., van Mulbregt, P., SciPy 1.0 Contributors, 2020. SciPy 1.0: Fundamental Algorithms for Scientific Computing in Python. Nature Methods 17, 261–272. doi:10.1038/s41592-019-0686-2.

Wilk, S., 2024. Lateral Track Strength Increase during Maintenance Speed Restrictions. Technical Report TD24-003. MxV Rail. URL: https://www.mxvrail.com/technology-digest/

lateral-track-strength-increase-during-maintenance-speed-restrictions/. technology Digest.

Wilk, S., Li, D., Gao, Y., Johnson, C., 2024. FAST Baseline Ballast and Subgrade Characterization. Technical Report. MxV Rail. Technology Digest.

Yang, G., Bradford, M.A., 2016. Thermal-induced buckling and postbuckling analysis of continuous railway tracks. International Journal of Solids and Structures 97, 637–649.